ChemPubSoc
Europe

Single-Molecule Metal-Induced Energy Transfer (smMIET): Resolving Nanometer Distances at the Single-Molecule Level

Narain Karedla, Alexey I. Chizhik, Ingo Gregor, Anna M. Chizhik, Olaf Schulz, and Jörg Enderlein*[a]

We present a new concept for measuring distance values of single molecules from a surface with nanometer accuracy using the energy transfer from the excited molecule to surface plasmons of a metal film. We measure the fluorescence lifetime of individual dye molecules deposited on a dielectric spacer as a function of a spacer thickness. By using our theoretical model, we convert the lifetime values into the axial distance of individual molecules. Similar to Förster resonance energy transfer (FRET), this allows emitters to be localized with nanometer accuracy, but in contrast to FRET the distance range at which efficient energy transfer takes place is an order of magnitude larger. Our technique can be potentially used as a tool for measuring intramolecular distances of biomolecules and complexes.

1. Introduction

Single-molecule detection and single-molecule spectroscopy have revolutionized the field of fluorescence microscopy. The number of techniques and methods based on single-molecule measurements has grown fast since its establishment in the late 20th century,[1] due to the enormous potential of being able to study physics, chemistry, and biology at the molecular level.[2]

One of the recent additions to the pool of single-molecule fluorescence tools are super-resolution imaging methods based on single-molecule localization. The most prominent methods are photo-activated localization microscopy (PALM),[3] and stochastic optical reconstruction microscopy (STORM),[4] or direct STORM (dSTORM).[5] The core idea is to label a sample with photo-switchable fluorescent molecules and then to take many consecutive images with different sub-sets of molecules switched into a fluorescent state in such a way that in each recorded image all fluorescing molecules are well separated from each other in space. Then these isolated molecules from each image are localized with an accuracy that is much superior to the optical resolution limit of the used microscope. In the end, by pooling together all positions of all detected molecules, a pointillistic super-resolved image is reconstructed.

The physical basis of these methods is the ability to pinpoint the position of an emitting molecule with much higher accuracy than the size of its image on the detector, that is, the point-spread function (PSF) of the microscope.[6] This lateral localization accuracy depends on the number of photons recorded

from the single molecule, among various other factors, and is given by Equation (1):[6]

$$\sigma_{xy} = \frac{\sigma_{PSF}^2}{N}\left(\frac{16}{9} + \frac{8\pi\sigma_{PSF}^2 b^2}{Na^2}\right) \tag{1}$$

in which σ_{xy} is the localization precision, σ_{PSF} is the full-width-at-half-maximum of the PSF, N is the number of photons collected from the molecule, b is the background noise level, and a is the pixel size of the detector. Under typical conditions, at room temperature, and by using conventional organic fluorophores, the achievable localization accuracy is around 20 nm laterally and thus is an order of magnitude better than the diffraction limit of resolution of a typical microscope. In addition, PALM, STORM, and dSTORM have found many applications in biological imaging with spectacular results; for example, see ref. [7]. By employing an astigmatism-based imaging scheme, these techniques have been used to study 3D ultrastructures in biological entities. However, the achievable resolution is still one order of magnitude worse than typical distances and sizes of biomacromolecules, which has prevented their wide application in structural biology on the macromolecular level, such as resolving the size and shape of gp210 proteins that surround and anchor onto the nuclear pore complexes (NPCs).[8] Moreover, the maximum achievable axial resolution in these techniques using the astigmatism approach is limited to 50 nm.

When it comes to sizes of few nanometers, the most used fluorescence-based optical method is still Förster resonance energy transfer (FRET),[9] named after its discoverer Theodor Förster.[10] FRET is based on the dipole–dipole coupling of two fluorophores, the so-called donor and acceptor. The electric near-field of the emitting donor falls off as r^{-3}, so the excitation efficiency of the acceptor follows a r^{-6} relationship. Due to this strong fall off on a nanometer length scale, FRET is used

[a] N. Karedla, Dr. A. I. Chizhik, Dr. I. Gregor, Dr. A. M. Chizhik, Dr. O. Schulz, Prof. Dr. J. Enderlein
Georg-August-Universität
III. Institute of Physics—Biophysics
Friedrich-Hund-Platz 1, 37077 Göttingen (Germany)
Fax: (+ 49) 551-39 7720
E-mail: enderlein@physik3.gwdg.de

as a molecular ruler.[11] Quantitatively, the rate of energy transfer from donor to acceptor is given by Equation (2):

$$k_a = \frac{1}{\tau_d}\left(\frac{R_0}{r}\right)^6 \tag{2}$$

in which τ_d is the donor's unperturbed fluorescence lifetime, r is the distance between donor and acceptor, and R_0 is the so-called Förster radius that depends on the donor's emission wavelengths, the absorption cross-section of the acceptor dipole at these wavelengths, and the relative orientation of both molecules to each other. It lies in the range of 2 to 6 nm. Single-pair FRET (spFRET) experiments were first realized by Ha et al.[12] They used near-field scanning optical microscopy (NSOM) on immobilized short DNA fragments with attached FRET pairs. Subsequently, many studies have successfully used spFRET for studying biological problems on the single-molecule level; for example, see refs. [13–21].

As powerful as FRET and spFRET are, they have two major limitations. First, the Förster radius critically depends on the relative orientation between donor and acceptor[17,22] For example, in the extreme case in which the donor's emission dipole is perpendicular to the acceptor's absorption dipole and both dipoles are orthogonal to the connecting line between donor and acceptor, the energy transfer efficiency is zero (at least in the dipole–dipole approximation). Usually, one assumes that both donor and acceptor are flexibly linked to the molecule of interest so that their orientation quickly changes during the excited state lifetime of the donor, which allows for quantitatively calculating the correct Förster radius. Unfortunately, if this assumption is not true, there is no independent measurement that could determine the full relative orientation between donor and acceptor. In that case, there is no way to correctly evaluate a FRET measurement and to extract quantitative and correct values for the distance between donor and acceptor. The second severe limitation is the short-distance range over which FRET is applicable. Due to the rapid fall off in energy-transfer efficiency with distance, one cannot usually measure distances beyond 10 nm.

Herein, we propose an alternative approach and present the first single-molecule study for measuring distances in the range of up to approximately 100 nm with nanometer precision. It opens new perspectives for overcoming both the limitations of FRET and the current resolution limitations of image-based single-molecule localization. The method is based on the energy transfer from an excited fluorescent molecule to surface plasmons in a thin metallic film and is thus called single-molecule metal-induced energy transfer (smMIET). This in turn modifies the excited-state lifetime of the emitting molecule. The theoretical basis of this effect has been worked out decades ago by Chance, Prock, and Silbey.[23] In particular, the change in lifetime depends on 1) the dipole's distance from the surface, 2) its orientation with respect to the surface, and 3) its intrinsic quantum yield. As a net result, the lifetime varies nonlinearly but monotonically with the dipole's distance from the metal surface over a range from 0 up to approximately 100 nm. Thus, one can use this monotonic lifetime–distance re-

lation for converting the measured lifetime value into the distance of the emitter from the surface. One prerequisite for doing that is a perfect theoretical understanding of the coupling between the emitting dipole and the metal.

Experimentally, Drexhage showed the influence of a mirror on a monolayer of phosphorescent europium complex molecules in the early 70s.[24] The model to explain the variation in emission rates was based on interference of a dipole's radiation with its mirror reflection. The disagreement of the model with the experiment at short distances is due to the transfer of energy from the europium complexes to the surface plasmons on a metal surface, which was later shown experimentally by Amos et al.[25] Lieberherr et al. also performed many experiments to show the variation in emission rates of a monolayer of molecules adsorbed on surfaces with different dielectric properties.[26] The core idea behind these experiments was to vary the dielectric constant of the environment by varying the distance between the emitter and the metal surface and obtain information regarding their radiative and nonradiative transition rates. The decay curves measured in such a manner can be used to extract the absolute values of quantum yields of luminescent molecules.[27,28] The first set of experiments demonstrating the possibility of exciting and detecting single fluorescent molecules through a thin metal film were performed by Stefani et al.,[29] who used annular beams with high NA objectives to excite single molecules placed at known distances from the metal surface.

In an earlier publication, we have already successfully employed MIET for measuring the distance of multiply labeled microtubules from a gold-covered surface with nanometer accuracy.[30] Recently, MIET was also used for nanoprofiling the basal membrane of living cells over a metal surface.[31] Herein we present the first experiments with MIET for localizing single molecules axially from a surface. The presented data show that smMIET indeed has the capacity of measuring distances of individual molecules from a surface with nanometer accuracy.

2. Theory

The near-field coupling of an emitting electric dipole (fluorescing molecule) and a planar multilayered substrate has been described many times in several publications, see for example, refs. [32–34]. In short, the emitting molecule is considered as an ideal oscillating electric dipole. To study the interaction of such a dipole with a planar structure, the emitted electromagnetic field of this dipole is mathematically represented by a superposition of plane waves. For each plane wave, the interaction with the planar substrate is calculated by using standard Fresnel theory, which in the end gives the desired full electromagnetic field of the emitter in the presence of the planar substrate. Finally, by integrating the Poynting vector of a given surface, one can then calculate the total energy flux of the emitted field through the given surface. This can be used to find the full emission rate of the emitting dipole and the part of the energy that is absorbed by the substrate (if it is not purely dielectric, e.g. metallic).

From these calculations, the emission rate $S(\theta,z)$ of an ideal electric dipole is given by Equation (3):

$$S(\theta,z) = S_\perp(z)\cos^2\theta + S_\parallel(z)\sin^2\theta \qquad (3)$$

in which θ is the angle between the dipole axis and the vertical (normal to the surface), z is the distance between the dipole and the surface, and the functions $S_\perp$ and $S_\parallel$ depend only on the distance z but not on the orientation θ. The ratio between this emission rate $S(\theta,z)$ and the emission rate of the free dipole (far away from the surface) S_0 describes the enhancement of the radiative transition of a molecule at distance z from the substrate with emission dipole orientation θ in the presence of the substrate. However, real fluorophores also exhibit nonradiative transitions from the excited to the ground state. If we denote the radiative transition rate by k_r and the nonradiative transition rate by k_{nr}, then the quantum yield of the fluorophore is defined by Equation (4):

$$\phi = k_r/(k_r+k_{nr}) \qquad (4)$$

and is equal to the chance that a molecule will emit a photon upon return to the ground state, and the fluorescence lifetime is given by the inverse total excited-to-ground-state transition rate [Eq. (5)]:

$$\tau = 1/(k_r+k_{nr}) \qquad (5)$$

Thus, when comparing the fluorescence lifetime between a free molecule far away from the substrate and a molecule at a distance z above the substrate, we find Equation (6):

$$\frac{\tau_0}{\tau(\theta,z)} = \frac{k_r(\theta,z)+k_{nr}}{k_{r,0}+k_{nr}} = \frac{S(\theta,z)}{S_0}\phi + 1 - \phi \qquad (6)$$

The obtained data (average lifetime as a function of distance z) are fitted with Equation (6) by using the angle θ and the free lifetime τ_0 as fit parameters, whereas the quantum yield value ϕ was taken from the literature.

3. Results and Discussion

Figure 1, left, shows an image of fluorescing single molecules deposited on a silicon oxide layer (30 nm thick) above a thin metal film (2 nm titanium, 10 nm gold) on a glass cover slide. The image was taken by using a confocal laser scanning microscope (for details, see the Experimental Section). The shown area is 30×30 μm². The background that can be seen on the image is due to the spectrally broad photoluminescence from the gold. However, the photoluminescence lifetime of a smooth gold surface is less than 2 ps, which does not affect the result of the measurement.[35] By applying a pattern-matching algorithm,[36] individual molecules are identified in the intensity image, as displayed in Figure 1, right. We repeated the measurements for four different values of SiO₂ spacer thickness, and the recorded fluorescence lifetime images are shown in Figure 2, in which we have already used the identified mole-
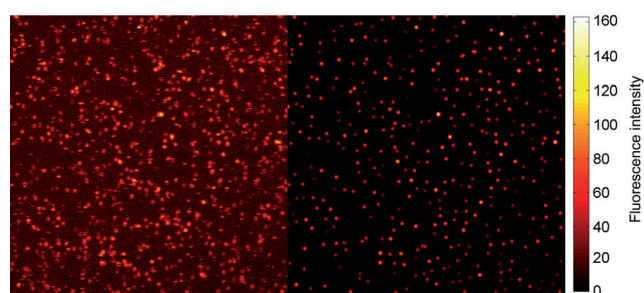

Figure 1. Left: Intensity image obtained from experiment. Right: Back-calculated image displaying all single molecules identified from the intensity image. The image size is 30×30 μm².
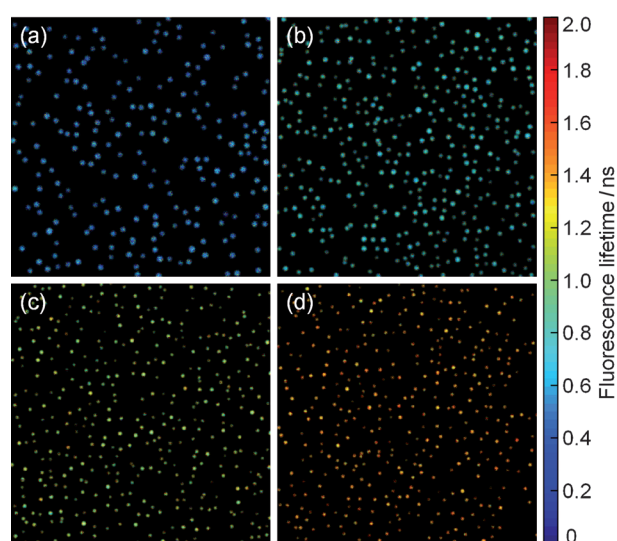

Figure 2. Lifetime images for a) 20, b) 30, c) 40, and d) 50 nm SiO₂ spacer thicknesses for the identified single-molecule pixels. The color bar shows the color index for lifetime values in nanoseconds. Each image is 30×30 μm²

cule positions to suppress any background that does not belong to individual molecule fluorescence. For each spacer thickness, we calculated the distribution of single-molecule lifetimes, as shown in Figure 3. The obtained lifetime values are (0.50 ± 0.06), (0.81 ± 0.07), (1.19 ± 0.08), and (1.50 ± 0.08) ns for 20, 30, 40, and 50 nm spacer thicknesses, respectively.

Emission rates $S_\perp(z)$ and $S_\parallel(z)$ were calculated for heights varying from 0 to 100 nm from the metal surface by using the bulk refractive indices for gold and titanium at $\lambda=684$ nm taken from the literature:[37] $n_{Au}=0.1706+3.7399i$ and $n_{Ti}=2.1648+3.2552i$. The value for the quantum yield of the used dye (Atto655) was set to 0.3 as provided by the manufacturer. By using the calculated emission rates as a function of distance, the experimental lifetime values were fitted to Equation (6) with free-space lifetime τ_0 and angle θ (which indicates the ratio of horizontal to vertical dipoles) as fit parameters. Figure 4 shows the fitted data along with curves of the lifetime modulation for purely horizontally and purely vertically oriented dipoles. The shaded area in between these two curves indicates the possible lifetime values for dipoles with polar orientations in between the two extremes. From the fit we find that
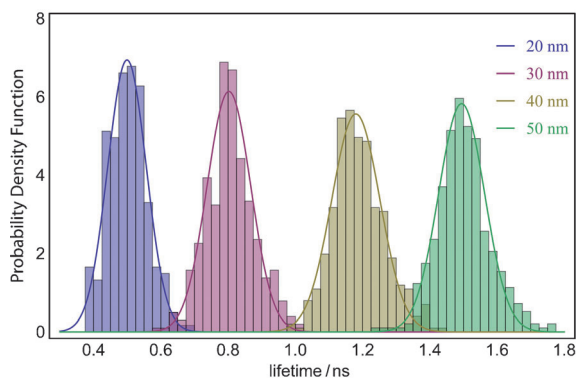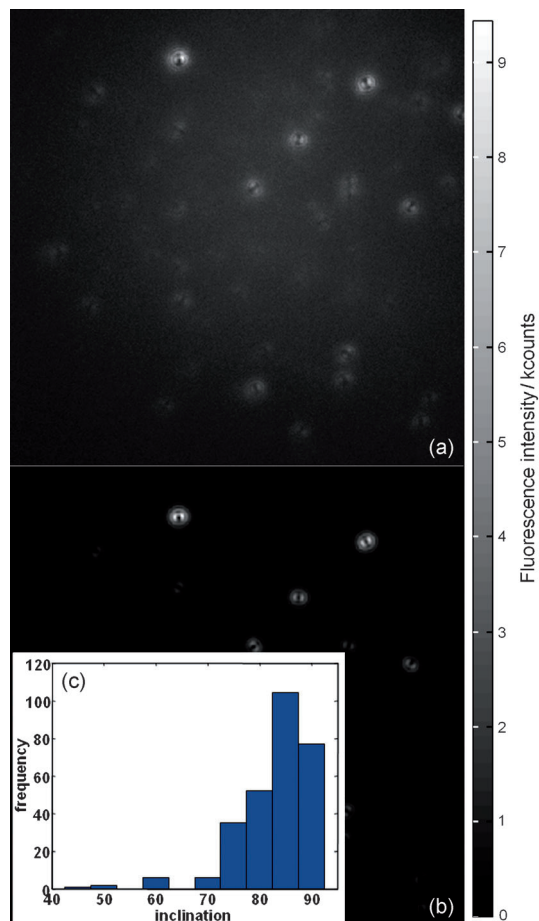
Figure 3. Lifetime distributions for the four samples with 20, 30, 40, and 50 nm SiO_2 spacers between the metal film and the deposited molecules.
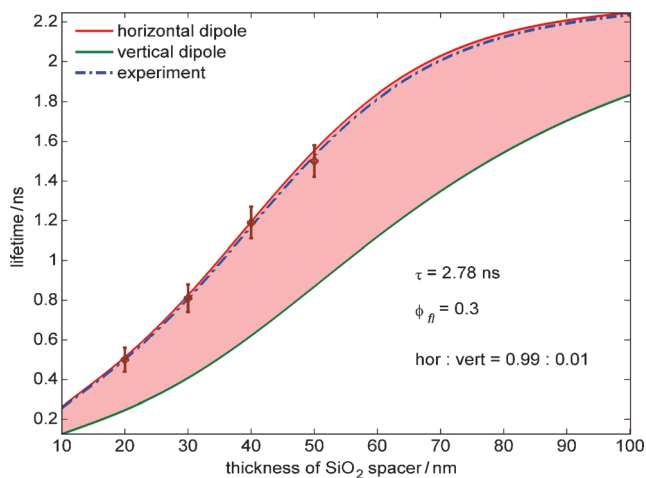
Figure 4. Fitting of experimental lifetime values by using Equation (6). The unperturbed lifetime τ_0 obtained as a fit parameter is 2.78 ns, which is in good agreement with the lifetime of Atto655 measured in air on glass.[39]

Figure 5. a) Measured defocused image of Atto655 single molecules on a silica spacer (20 nm) evaporated on a glass coverslip. The image (512×512) was obtained by moving the focus of the objective 0.85 μm above the substrate/air interface. b) The identified single-molecule patterns from the image in a) obtained by pattern matching after background subtraction. c) Histogram showing the single-molecule inclinations obtained by pattern matching analysis for 25 images taken from different areas in the sample with the same defocusing value.

the observed lifetime–distance behavior is best described if it is assumed that almost all molecules are horizontally oriented, which is expected for dye molecules that are spin-coated from solution onto a flat surface.[38]

Several defocused images of Atto655 single molecules were taken to get further orientation information. These measurements were performed on samples prepared by spin-coating Atto655 on a thin SiO_2 layer (20 nm) evaporated on glass coverslips. All the images were acquired with an exposure time of about 10 s with total internal reflection (TIR) illumination. The focus of the objective was moved to about 1 μm above the substrate/air interface to acquire the image. The camera was operated at −80 °C, a preamp gain of 3.7, and an EM gain of 5 to 10 depending on the brightness of the molecules. Figure 5a shows the defocused patterns of around 20 single molecules on a CCD area of 512×512 pixels with an effective pixel size of 80 nm. Model patterns for various orientations and defocusing values were calculated according to the theory given by Patra et al.[36] To estimate the correct value of defocusing, we compared the computed patterns with the patterns obtained in the image for horizontal dipoles for various values of defocus-

ing. Because the horizontal dipole pattern at the silica/air boundary is highly sensitive to the defocusing level, the correct value can be estimated to within ±0.3 μm. For the image shown in Figure 5a, the defocusing value was estimated to be +0.85 μm. We then calculated the theoretical patterns of defocused dipoles oriented at 826 different orientations in space (not shown here). These patterns were calculated by individually varying the azimuthal angle (in-plane) and the polar angle (out-of-plane) by 5°. The radius for computing the patterns was chosen as 20 pixels. These model patterns were then used to match to the defocused images obtained by using a custom Matlab routine. With such an analysis, the orientations of single molecules can be identified with a resolution of 5° in 3D. Figure 5b shows the identified patterns of 18 single molecules. Such a pattern matching algorithm was carried out on 25 different defocused images, for the same defocusing value, to obtain a histogram of inclinations for the single molecules, shown in Figure 5c. The histogram accounts for 268 patterns that have inclinations ≥75° out of 283 identified pat-

terns. The fitting accuracy depends dramatically on the signal-to-noise (S/N) ratio of the defocused patterns. Poor S/N can bring down the resolution for determining the polar angles to as low as 20°, which is the case for most of the defocused patterns obtained in our images (see Figure 5a). Within these limitations, the result obtained from the distribution of single-molecule inclinations is in good agreement with our fitting result obtained above (Figure 4) for estimating the percentage of horizontal dipoles.

The values of the fit parameters for Equation (6), that is, the unperturbed lifetime of the dipole and the ratio between horizontal and vertical dipoles, depend on the quantum yield value, which we take as 30%. A slight reduction in the quantum yield, which can be the situation for single molecules at the air/silica interface, shifts the shaded area in Figure 4 to higher lifetime values and thereby changes the ratio of horizontal to vertical dipoles. For example, if the quantum yield was taken as 29%, the ratio changes to 94:6, whereas the unperturbed lifetime value rises to 2.85 ns.

The standard deviation for the observed single-molecule lifetime values is less than 0.1 ns, which corresponds to an axial localization accuracy of less than 2.5 nm for horizontal dipoles. A further reduction in the spread of the lifetime distribution can be achieved by increasing the number of collected photons per molecule, for example, by preventing photobleaching by using suitable oxygen-scavenging protocols.[40] In our current experiment, we detected on average 369, 767, 1002, and 1031 photons per identified molecule for spacer thickness values of 20, 30, 40, and 50 nm, respectively.

In our current measurement scheme, the fundamental limitation is that we have no means of measuring the orientation (polar angle) of the molecule simultaneously with the intensity and lifetime. As can be seen from Figure 4, the relation between distance and lifetime is strongly orientation dependent and to use smMIET for nanometer-precise distance measurements of single molecules, one will need to know both the lifetime and the orientation. There are several options to achieve this, including defocused imaging[41, 36] scanning with radially polarized light,[42] or detecting separately sub- and supercritical fluorescence emission.[43] However, all these methods require significant extensions and/or modifications of a conventional confocal laser scanning microscope, and future investigations must be made to determine which of these methods is the most robust and efficient in terms of extracted information per detected photon.

4. Conclusion and Outlook

We have presented the concept of smMIET, which uses fluorescence lifetime information to determine the distance between a single molecule and a metallized surface. The physical basis behind smMIET is the energy transfer from the excited molecule to surface plasmons in the metal and is thus quite similar to FRET. As in the case of FRET, it also needs information about the orientation of the emitting molecule. However, the distance range over which smMIET works is much larger than FRET. In the case of smMIET, only the vertical orientation of the

emission dipole with respect to the surface is needed whereas in FRET, three relative orientation angles between donor emission and acceptor absorption dipoles are needed, which are inaccessible by using any independent measurement.

In combination with orientation measurements, smMIET can determine distance values of single molecules from a surface with nanometer resolution. Already with our nonoptimized (in terms of photobleaching) measurements we could estimate a positional accuracy of better than 2.5 nm. Although smMIET achieves this resolution only along one single axis, this method will open new fascinating possibilities for structural biology. For example, for determining the intramolecular distance between two fluorescent labels in a macromolecule, one can envision using smMIET to measure the absolute distance values of both labels for a large number of macromolecules immobilized on a surface. One could then apply a statistical analysis of the acquired distance histograms to obtain the absolute distance between the labels.

Experimental Section

Cleaned glass coverslips (thickness 150 μm, refractive index 1.52) were used as substrates for vapor deposition of 2 nm titanium and 10 nm gold and SiO_2 spacer of required thickness (20, 30, 40, 50 nm in the order mentioned). The process was carried out under high-vacuum conditions ($\approx 10^{-6}$ mbar) by using an electron beam source (Univex 350, Leybold). The slowest rate of deposition was maintained (1 Å s^{-1}) to ensure maximum smoothness on the surface. The thickness of the layers was monitored by using an oscillating quartz unit during deposition and later verified by using atomic force microscopy. Atto655 (Atto Tech) was diluted to 1 nM in Millipore water (18.2 MΩ cm at 25 °C). An aliquot of this solution (10 μL) was spin-coated onto the substrates prepared at 8000 rpm for 40 s. This dye was used mainly due its reported good photostability in air and long lifetime of around 3.0 ns.[39]

For lifetime imaging, the commercial confocal system Microtime 200 (PicoQuant, Berlin, Germany) was used. Figure 6 depicts a schematic of the setup, which contains four basic parts:
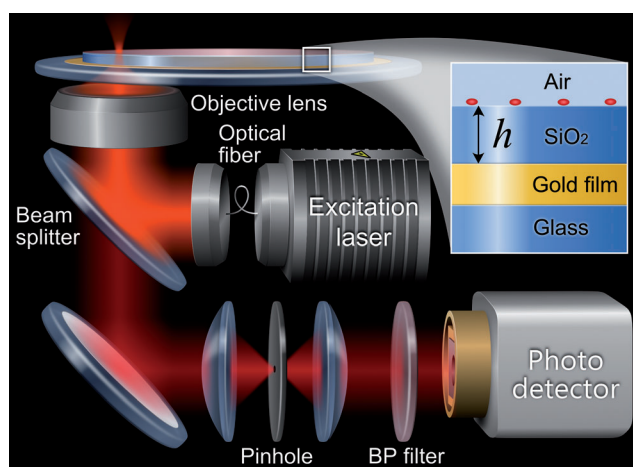

Figure 6. Illustration of the setup. Inset: The geometry of the substrate.

1) The microscope: A modified Olympus IX-71 microscope (Olympus Deutschland, Hamburg, Germany) with an accessible standard side port on the right side was used. The samples were scanned at a speed of 4–6 ms per 67 nm pixel by using a three-axis piezo stage (P-562.3CD, Physical Instruments) that was driven with a digital piezo controller (E-710 Physical Instruments).

2) The excitation system: A pulsed diode laser ($\lambda = 640$ nm, LDH-D-C-640, PicoQuant) with a pulse width of 100 ps full-width at half-maximum was operated at a pulsing frequency of 40 MHz by using a multichannel picosecond diode laser driver (PDL 828 "Sepia II"; PicoQuant). A clean-up filter (Z640/10X, Chroma Technology) was used to block unwanted wavelengths from the laser. The laser beam was then coupled to a polarization-maintaining single-mode optical fiber (PMC-400-4.2-NA010-3-APC-250 V, Schäfter and Kirchhoff, Germany).

3) The main optical unit: The fiber output was collimated to a beam of 9 mm diameter by coupling it to an infinity-corrected 4× objective (UPLSAPO4X, Olympus). The excitation beam was then reflected by using a dichroic mirror (FITC/CY5 (51008bs), Chroma Technology) to guide it into the side port of the microscope. The excitation power used was around 10–25 kW cm^{-2}. A high numerical aperture objective was used to excite the samples (UAPON 100XOTIRF, 1.49 N.A., Olympus) and to collect the fluorescence emission. The emission light was then passed through the dichroic mirror and focused onto a 50 μm pinhole for confocal imaging. After the pinhole it was refocused by using a pair of achromatic lens doublets onto the active area (≈ 75 μm) of a single-photon counting module (SPCM-AQR-13, Perkin–Elmer, $\approx 70\%$ quantum yield of detection at $\lambda = 670$ nm). A band-pass filter (BrightLine HC 692/40, Semrock) was used before the detector to block the back-scattered laser light and a major part of gold photoluminescence. The dark count rate of the detector was less than 150 counts s^{-1}.

4) Data acquisition and processing: The transistor-transistor-logic (TTL) pulses from the SPCM were recorded with a 2 ps time resolution by using a multichannel picosecond event timer and time-correlated single-photon counting (TCSPC) module (HydraHarp 400, PicoQuant) in the time-tagged time-resolved (TTTR) acquisition mode.[44] The periodic sync signal for the time gates was obtained from the Sepia II driver. The collected photon data was processed by using the commercial software SymPhoTime v.5.2 (PicoQuant) to obtain intensity and lifetime images. Pixels corresponding to single molecules were identified from this intensity image by using a custom Matlab routine. A weighted average of pixel lifetime values with intensity values as their weights was calculated separately for each single molecule. Finally, a histogram of average lifetimes of all the identified single molecules in the image was plotted.

For defocused imaging, substrates were prepared by evaporating 20 nm SiO$_2$ onto cleaned glass coverslips without any gold layer. Atto655 (50 pM) was then spin-coated onto these substrates. An EMCCD Camera (iXon+ DU-885 K, Andor Technology, Ireland, with 1004×1002 pixels and 8×8 μm^2 pixel size) was coupled to the trinocular observation tube of an Olympus IX-71 microscope (Olympus Deutschland). For excitation, a $\lambda = 647$ nm diode laser (PhoxX 647, 140 mW, Omicron Laserage, Germany) was modulated by using the "Fire" output of the camera. The linearly polarized laser beam was focused on the back aperture of the objective (UAPON 100XOTIRF, 1.49 N.A., Olympus). The focused beam was shifted across the back aperture by using a movable mirror to illuminate the sample in TIR mode with an average illumination power of 0.2 kW cm^{-2}. The emission light was collected by using the same objective and passed through a dichroic mirror (Di01-R405/488/561/635-25×36, Semrock) and further filtered by using a quad-band pass filter (FF01-446/523/600/677, Semrock) before it was focused onto the camera chip.

Acknowledgements

[1] W. E. Moerner, L. Kador, *Anal. Chem.* **1989**, *61*, 1217A–1223A.
[2] T. Plakhotnik, E. A. Donley, U. P. Wild, *Annu. Rev. Phys. Chem.* **1997**, *48*, 181–212.
[3] E. Betzig, G. H. Patterson, R. Sougrat, O. W. Lindwasser, S. Olenych, J. S. Bonifacino, M. W. Davidson, J. Lippincott-Schwartz, H. F. Hess, *Science* **2006**, *313*, 1642–1645.
[4] M. J. Rust, M. Bates, X. Zhuang, *Nat. Methods* **2006**, *3*, 793–795.
[5] M. Heilemann, S. van De Linde, M. Schüttpelz, R. Kasper, B. Seefeldt, A. Mukherjee, P. Tinnefeld, M. Sauer, *Angew. Chem. Int. Ed.* **2008**, *47*, 6172–6176; *Angew. Chem.* **2008**, *120*, 6266–6271.
[6] K. I. Mortensen, L. S. Churchman, J. A. Spudich, H. Flyvbjerg, *Nat. Methods* **2010**, *7*, 377–381.
[7] K. Xu, G. Zhong, X. Zhuang, *Science* **2013**, *339*, 452–456.
[8] A. Löschberger, S. van de Linde, M.-C. Dabauvalle, B. Rieger, M. Heilemann, G. Krohne, M. Sauer, *J. Cell Sci.* **2012**, *125*, 570–575.
[9] R. M. Clegg, in *Fluorescence Imaging Spectroscopy and Microscopy* (Eds.: X. F. Wang, B. Herman), John Wiley & Sons, New York, **1996**, pp. 179–252.
[10] T. Förster, *Annalen der Physik* **1948**, *437*, 55–75.
[11] J. Zheng in *Biomedical Applications of Biophysics SE - 5* (Ed.: T. Jue), Humana Press, **2010**, pp. 119–136.
[12] T. Ha, T. Enderle, D. F. Ogletree, D. S. Chemla, P. R. Selvin, S. Weiss, *Proc. Natl. Acad. Sci. USA* **1996**, *93*, 6264–6268.
[13] B. Schuler, W. A. Eaton, *Curr. Opin. Struct. Biol.* **2008**, *18*, 16–26.
[14] R. Roy, S. Hohng, T. Ha, *Nat. Methods* **2008**, *5*, 507–516.
[15] N. K. Lee, A. N. Kapanidis, Y. Wang, X. Michalet, J. Mukhopadhyay, R. H. Ebright, S. Weiss, *Biophys. J.* **2005**, *88*, 2939–2953.
[16] E. Nir, X. Michalet, K. M. Hamadani, T. Laurence, D. Neuhauser, Y. Kovchegov, S. Weiss, *J. Phys. Chem. B* **2006**, *110*, 22103–22124.
[17] A. K. Wozniak, G. F. Schröder, H. Grubmüller, C. A. M. Seidel, F. Oesterhelt, *Proc. Natl. Acad. Sci. USA* **2008**, *105*, 18337–18342.
[18] C. A. M. Seidel, S. Kalinin, S. Felekyan, A. Valeri, S. Sindbert, *Biophys. J.* **2010**, *98*, 266a–266a.
[19] S. Kalinin, E. Sisamakis, S. W. Magennis, S. Felekyan, C. A. M. Seidel, *J. Phys. Chem. B* **2010**, *114*, 6197–6206.
[20] Y. Gambin, A. A. Deniz, *Mol. Biosyst.* **2010**, *6*, 1540–1547.
[21] E. Sisamakis, A. Valeri, S. Kalinin, P. J. Rothwell, C. A. M. Seidel, *Methods* **2010**, *475*, 455–514.
[22] A. Muschielok, J. Andrecka, A. Jawhari, F. Bruckner, P. Cramer, J. Michaelis, *Nat. Methods* **2008**, *5*, 965–971.
[23] R. R. Chance, A. Prock, R. Silbey, *Adv. Chem. Phys.* **1978**, *37*, 1–65.
[24] K.-H. Drexhage, *Prog. Optics* **1974**, *12*, 163.
[25] R. M. Amos, W. L. Barnes, *Phys. Rev. B* **1997**, *55*, 7249–7254.
[26] M. Lieberherr, Ch. Fattinger, W. Lukosz, *Surf. Sci.* **1987**, *189/190*, 954–959.
[27] B. C. Buchler, T. Kalkbrenner, C. Hettich, V. Sandoghdar, *Phys. Rev. Lett.* **2005**, *95*, 063003.

[28] A. I. Chizhik, A. M. Chizhik, D. Khoptyar, S. Bär, A. J. Meixner, J. Enderlein, *Nano Lett.* **2011**, *11*, 1700–1703.

[29] F. D. Stefani, K. Vasilev, N. Bocchio, N. Stoyanova, M. Kreiter, *Phys. Rev. Lett.* **2005**, *94*, 023005.

[30] M. Berndt, M. Lorenz, J. Enderlein, S. Diez, *Nano Lett.* **2010**, *10*, 1497–1500.

[31] A. I. Chizhik, J. Rother, I. Gregor, A. Janshoff, J. Enderlein, *Nature Photon.* **2013**, DOI: 10.1038/nphoton.2013.345

[32] J. Enderlein, *Chem. Phys.* **1999**, *247*, 1–9.

[33] J. Enderlein, *Biophys. J.* **2000**, *78*, 2151–2158.

[34] A. I. Chizhik, I. Gregor, B. Ernst, J. Enderlein, *ChemPhysChem* **2013**, *14*, 505–513.

[35] M. Beversluis, A. Bouhelier, L. Novotny, *Phys. Rev. B* **2003**, *68*, 115433.

[36] D. Patra, I. Gregor, J. Enderlein, *J. Phys. Chem. A* **2004**, *108*, 6836–6841.

[37] A. D. Rakić, A. B. Djurišić, J. M. Elazar, M. L. Majewski, *Appl. Opt.* **1998**, *37*, 5271–5283.

[38] X. S. Xie, R. C. Dunn, *Science* **1994**, *265*, 361–364.

[39] O. Schulz, Z. Zhao, A. Ward, M. Koenig, F. Koberling, Y. Liu, J. Enderlein, H. Yan, R. Ros, *Opt. Nanosc.* **2013**, *2*, 1.

[40] J. Vogelsang, R. Kasper, C. Steinhauer, B. Person, M. Heilemann, M. Sauer, P. Tinnefeld, *Angew. Chem. Int. Ed.* **2008**, *47*, 5465–5469; *Angew. Chem.* **2008**, *120*, 5545–5550.

[41] M. Böhmer, J. Enderlein, *J. Opt. Soc. Am. A J. Opt. Soc.Am.B* **2003**, *20*, 554–559.

[42] A. I. Chizhik, A. M. Chizhik, D. Khoptyar, S. Bär, A. J. Meixner, *Nano Lett.* **2011**, *11*, 1131–1135.

[43] J. Hohlbein, C. G. Hübner, *J. Chem. Phys.* **2008**, *129*, 094703.

[44] M. Wahl, H.-J. Rahn, T. Röhlicke, G. Kell, D. Nettels, F. Hillger, B. Schuler, R. Erdmann, *Rev. Sci. Instrum.* **2008**, *79*, 123113.